

# A Strong Form Meshfree Collocation Method: Engineering Applications Including Frictional Contact



Tae-Yeon Kim, Jeong-Hoon Song, and Tod A. Laursen

*This article is dedicated to my friend and longtime colleague Peter Wriggers on his 70th birthday. We were first introduced by my doctoral advisor Juan Simo on the Stanford campus in 1990, and I have been so pleased and privileged to collaborate with Peter on so many things, including organization of conferences and minisymposia, short courses, and various publication projects throughout the years. Thank you Peter for your friendship, your generosity, and your mentorship over the course of my career, and my very best wishes for health, happiness, and continued productivity in the years to come (T. Laursen).*

**Abstract** This article provides the brief review of the recently developed strong form meshfree collocation method. The method directly discretizes a strong form with approximated derivatives from the moving least-squares approximation using the Taylor polynomial of the unknown variable. The approximations of derivatives of any order can be generated in the process of computing the shape function without further cost. The method does not require mesh structure and numerical integration, and adaptivity can be easily achieved by locally refining collocation points. The discretization of the strong form using the derivative approximation is briefly described based on a frictional contact problem. Moreover, recent applications and developments of the method for various engineering problems are briefly presented.

---

T.-Y. Kim

Department of Civil Infrastructure and Environmental Engineering, Khalifa University of Science and Technology, Abu Dhabi, UAE

e-mail: [taeyeon.kim@ku.ac.ae](mailto:taeyeon.kim@ku.ac.ae)

J.-H. Song

Department of Civil, Environmental and Architectural Engineering, University of Colorado at Boulder, Boulder, CO, USA

e-mail: [jh.song@colorado.edu](mailto:jh.song@colorado.edu)

T. A. Laursen (✉)

Department of Civil, Structural and Environmental Engineering, University at Buffalo, Buffalo, NY, USA

e-mail: [Tod.Laursen@suny.edu](mailto:Tod.Laursen@suny.edu)

# 1 A Strong Form Meshfree Collocation Method

The strong form meshfree collocation method is based on the idea of Kim and Kim [1] and Yoon and Song [2–4]. The method discretizes directly a strong form with the derivative approximation generated from the moving least-squares approximation using a Taylor expansion of the unknown variable. This section provides the brief procedure of constructing such derivative approximation. Further details can be found in [1–4].

## 1.1 Approximation of Derivative Operators

Let  $\mathbf{x} = (x_1, \dots, x_n)$  be an  $n$ -dimensional real vector and  $\boldsymbol{\alpha} = (\alpha_1, \dots, \alpha_n)$  be an  $n$ -tuple of non-negative integers. The  $\boldsymbol{\alpha}$ th-power of  $\mathbf{x}$  is defined by  $\mathbf{x}^\boldsymbol{\alpha} = x_1^{\alpha_1} x_2^{\alpha_2} \dots x_n^{\alpha_n}$ . The  $\boldsymbol{\alpha}$ th-order derivative of a smooth function  $f(\mathbf{x})$  with respect to  $\mathbf{x}$  is defined by

$$D_{\mathbf{x}}^{\boldsymbol{\alpha}} f(\mathbf{x}) = \frac{\partial^{|\boldsymbol{\alpha}|} f(\mathbf{x})}{\partial x_1^{\alpha_1} \partial x_2^{\alpha_2} \dots \partial x_n^{\alpha_n}} \quad (1)$$

where  $|\boldsymbol{\alpha}| = \sum_{i=1}^n \alpha_i$ .

The  $m$ th-order Taylor polynomial for approximating a function  $u(\mathbf{x})$  at the local center  $\bar{\mathbf{x}}$  can be expressed as

$$u(\mathbf{x}; \bar{\mathbf{x}}) = \sum_{|\boldsymbol{\alpha}| \leq m} \frac{(\mathbf{x} - \bar{\mathbf{x}})^{\boldsymbol{\alpha}}}{\boldsymbol{\alpha}!} D_{\mathbf{x}}^{\boldsymbol{\alpha}} u(\bar{\mathbf{x}}) = \mathbf{p}_m^T(\mathbf{x}; \bar{\mathbf{x}}) \mathbf{M}(\bar{\mathbf{x}}) \quad (2)$$

where  $\boldsymbol{\alpha}!$  is the factorial of  $\boldsymbol{\alpha}$  and the polynomial vector  $\mathbf{p}_m^T(\mathbf{x}; \bar{\mathbf{x}})$  and the derivative coefficient vector  $\mathbf{M}(\bar{\mathbf{x}})$  are defined by

$$\mathbf{p}_m^T(\mathbf{x}; \bar{\mathbf{x}}) = \left[ \frac{(\mathbf{x} - \bar{\mathbf{x}})^{\boldsymbol{\alpha}_1}}{\boldsymbol{\alpha}_1!}, \dots, \frac{(\mathbf{x} - \bar{\mathbf{x}})^{\boldsymbol{\alpha}_L}}{\boldsymbol{\alpha}_L!} \right], \quad \mathbf{M}^T(\bar{\mathbf{x}}) = [D_{\mathbf{x}}^{\boldsymbol{\alpha}_1} u(\bar{\mathbf{x}}), \dots, D_{\mathbf{x}}^{\boldsymbol{\alpha}_L} u(\bar{\mathbf{x}})], \quad (3)$$

in which  $\boldsymbol{\alpha}_i$ 's are an  $n$ -tuple of non-negative integers and  $L = (n + m)!/n!m!$  is the number of the components of  $\mathbf{p}_m^T$ .

Bearing in mind of the idea of the moving least-squares approximation, minimizing the discrete form of the weighted, discrete  $L_2$ -norm

$$\mathbf{J}(\mathbf{a}) = \sum_{l=1}^N w \left( \frac{\mathbf{x}_l - \bar{\mathbf{x}}}{\rho} \right) [\mathbf{p}^T(\mathbf{x}_l) \mathbf{M}(\bar{\mathbf{x}}) - u_l]^2 \quad (4)$$

with respect to  $\mathbf{M}(\bar{\mathbf{x}})$  yields

$$\mathbf{M}(\bar{\mathbf{x}}) = \mathbf{M}^{-1}(\bar{\mathbf{x}}) \mathbf{B}(\bar{\mathbf{x}}) \mathbf{u}^T. \quad (5)$$

The matrices  $\mathbf{M}$  and  $\mathbf{B}$  can be defined by

$$\mathbf{M}(\bar{\mathbf{x}}) = \sum_{I=1}^N w \left( \frac{\mathbf{x}_I - \bar{\mathbf{x}}}{\rho} \right) \mathbf{p}_m(\mathbf{x}_I; \bar{\mathbf{x}}) \mathbf{p}_m^T(\mathbf{x}_I; \bar{\mathbf{x}}), \quad (6)$$

$$\mathbf{B}(\bar{\mathbf{x}}) = \left[ w \left( \frac{\mathbf{x}_1 - \bar{\mathbf{x}}}{\rho} \right) \mathbf{p}_m(\mathbf{x}_1; \bar{\mathbf{x}}), \dots, w \left( \frac{\mathbf{x}_N - \bar{\mathbf{x}}}{\rho} \right) \mathbf{p}_m(\mathbf{x}_N; \bar{\mathbf{x}}) \right] \quad (7)$$

where  $w \left( \frac{\mathbf{x}_I - \bar{\mathbf{x}}}{\rho} \right)$  is the weight function with a compact support (or domain of influence) in which its size is determined by the dilation parameter  $\rho$ ,  $N$  is the number of nodes included in the support of the weight function, and  $u_I$  is the nodal solution for neighbor node  $I$ .

Substituting  $\mathbf{x}$  for  $\bar{\mathbf{x}}$  and replacing  $\mathbf{M}(\mathbf{x})$  with  $\mathbf{D}_{\mathbf{x}}^{\alpha} u(\mathbf{x})$  in (5) give rise to the  $\alpha$ th derivative approximation of  $u(\mathbf{x})$

$$\mathbf{D}_{\mathbf{x}}^{\alpha} u(\mathbf{x}) = \sum_{I=1}^N \Phi_I^{\alpha}(\mathbf{x}) u_I \quad (8)$$

where  $\alpha = (\alpha_1, \alpha_2)$  be a 2-tuple of non-negative integers and  $\Phi_I^{\alpha}(\mathbf{x})$  is the  $\alpha$ th-order derivative of the shape function at node  $I$  defined as

$$\Phi_I^{\alpha}(\mathbf{x}) = \mathbf{e}_{\alpha}^T \mathbf{M}^{-1}(\mathbf{x}) \mathbf{p}(\mathbf{x}_I; \mathbf{x}) w \left( \frac{\mathbf{x}_I - \mathbf{x}}{\rho} \right) \quad (9)$$

where  $\mathbf{e}_{\alpha}^T = [e_0, \dots, e_m]$  with its component defined as  $e_k = 1$  if  $k = \alpha$  and  $e_k = 0$  otherwise for  $k = 0, \dots, m$ .

It is worthwhile to mention that (8) does not require actual differentiation as shown in (9). As a consequence, this method doesn't require the regularity of the weight function to ensure the regularity of the shape functions.

## 1.2 Discretization of a Strong Form for Frictional Contact

The derivate approximation (8) allows for straightforward computation of derivative operators that can directly discretize a strong form of any order as well as their boundary conditions. We briefly provide the application of (8) to frictional contact problems by directly imposing contact constraints as part of Neumann boundary conditions on the elastostatic equation  $\nabla \cdot \boldsymbol{\sigma} + \mathbf{b} = 0$  with  $\boldsymbol{\sigma}$  being the Cauchy stress and  $\mathbf{b}$  the body force. Details are referred to as Almansi et al. [5].

Upon substituting the constitutive relation of  $\boldsymbol{\sigma}$  for linear elastic isotropic material, the elastostatic equation can be written in terms of the displacement  $\mathbf{u}$  as

$$\mu \Delta \mathbf{u} + (\lambda + \mu) \nabla (\nabla \cdot \mathbf{u}) + \mathbf{b} = 0 \quad \text{in } \Omega \quad (10)$$

where  $\lambda$  and  $\mu$  are Lamé constants. Similarly, Dirichlet and Neumann boundary conditions and contact constraints can be written as

$$\begin{aligned} \mathbf{u} &= \bar{\mathbf{u}} \quad \text{on } \Gamma_u, \\ 2\mu \mathbf{n} \cdot \boldsymbol{\epsilon} + \lambda \mathbf{n} \cdot \mathbf{1}(\nabla \cdot \mathbf{u}) &= \bar{\mathbf{t}} \quad \text{on } \Gamma_t, \\ 2\mu \mathbf{n} \cdot \boldsymbol{\epsilon} + \lambda \mathbf{n} \cdot \mathbf{1}(\nabla \cdot \mathbf{u}) &= \mathbf{t}_c \quad \text{on } \Gamma_c \end{aligned} \tag{11}$$

where  $\boldsymbol{\epsilon} = (\nabla \mathbf{u} + (\nabla \mathbf{u})^T)$  is the strain tensor,  $\mathbf{n}$  is the unit outward normal vector to domain  $\Omega$ ,  $\bar{\mathbf{u}}$  is the prescribed displacement on  $\Gamma_u$ ,  $\bar{\mathbf{t}}$  is the prescribed traction on  $\Gamma_t$ , and  $\mathbf{t}_c$  is the unknown contact traction on  $\Gamma_c$ .

By substituting (8) into (10), the discrete form of (10) can be obtained as

$$\begin{aligned} \sum_{I=1}^N \{[(\lambda + 2\mu)\Phi_{IJ}^{(2,0)} + \mu\Phi_{IJ}^{(0,2)}]u_{1I} + (\lambda + \mu)\Phi_{IJ}^{(1,1)}u_{2I}\} + b_{1J} &= 0, \\ \sum_{I=1}^N \{(\lambda + \mu)\Phi_{IJ}^{(1,1)}u_{1I} + [\mu\Phi_{IJ}^{(2,0)} + (\lambda + 2\mu)\Phi_{IJ}^{(0,2)}]u_{2I}\} + b_{2J} &= 0 \end{aligned} \tag{12}$$

where  $\mathbf{x}_J$  indicates interior nodes within  $\Omega$  and  $(\cdot)_J$  indicates the value at  $\mathbf{x}_J$ , e.g.,  $\Phi_{IJ}^{(2,0)} = \Phi_I^{(2,0)}(\mathbf{x}_J)$ . Similarly, the discrete forms of Dirichlet and Neumann boundary conditions at boundary nodes can be obtained by substituting (8) into (11)<sub>1</sub> and (11)<sub>2</sub> as shown in (4.23) and (4.26) in [5].

The contact traction can be decomposed into the normal and tangential components, i.e.,  $\mathbf{t}_c = \mathbf{t}_N - \mathbf{t}_T = t_N \mathbf{n}u - t_T \boldsymbol{\tau}$  where  $t_N$  and  $t_T$  are subject to the classical Kuhn-Tucker constraints governing contact interaction as in (3.4) and (3.7) of [5] and  $\mathbf{v}$  and  $\boldsymbol{\tau}$  are the unit normal and tangential vectors on  $\Gamma_c$ . For the normal contact constraint, the penalty regularization is achieved by  $t_N = \epsilon_N \langle g \rangle$  where  $\langle g \rangle$  is the Macaulay bracket of a gap function  $g$  and  $\epsilon_N$  is the normal penalty parameter. With the tangential penalty parameter  $\epsilon_T$ , the penalty regularization for frictional contact constraint can be constructed by (3.7) and (3.8) in [5] along with a trial state/return mapping algorithm to determine the Columb frictional traction as in (3.9) and (3.10) of [5]. Substituting (8) into (11)<sub>3</sub> results in the discrete forms of the contact constraints for both stick and slip as follows. For the stick case,

$$\begin{aligned} \sum_{I=1}^N \{[(\lambda + 2\mu)\Phi_{IJ}^{(1,0)}n_1 + \mu\Phi_{IJ}^{(0,1)}n_2]u_{1I} + [\lambda\Phi_{IJ}^{(0,1)}n_1 + \mu\Phi_{IJ}^{(1,0)}n_2]u_{2I}\} \\ - \epsilon_N \langle g(\mathbf{x}_J) \rangle v_1 + \epsilon_T H(g(\mathbf{x}_J))(\mathbf{u} \cdot \boldsymbol{\tau})\tau_1 &= 0, \\ \sum_{I=1}^N \{[\mu\Phi_{IJ}^{(0,1)}n_1 + \lambda\Phi_{IJ}^{(1,0)}n_2]u_{1I} + [(\lambda + 2\mu)\Phi_{IJ}^{(0,1)}n_2 + \mu\Phi_{IJ}^{(1,0)}n_1]u_{2I}\} \\ - \epsilon_N \langle g(\mathbf{x}_J) \rangle v_2 + \epsilon_T H(g(\mathbf{x}_J))(\mathbf{u} \cdot \boldsymbol{\tau})\tau_2 &= 0, \end{aligned} \tag{13}$$

and for the slip case,

$$\begin{aligned}
 & \sum_{I=1}^N \{[(\lambda + 2\mu)\Phi_{IJ}^{(1,0)} n_1 + \mu\Phi_{IJ}^{(0,1)} n_2]u_{1I} + [\lambda\Phi_{IJ}^{(0,1)} n_1 + \mu\Phi_{IJ}^{(1,0)} n_2]u_{2I}\} \\
 & \quad -\epsilon_N < g(\mathbf{x}_J) > v_1 + \mu\epsilon_N < g(\mathbf{x}_J) > \text{sign}(\mathbf{u} \cdot \boldsymbol{\tau})\tau_1 = 0, \\
 & \sum_{I=1}^N \{[\mu\Phi_{IJ}^{(0,1)} n_1 + \lambda\Phi_{IJ}^{(1,0)} n_2]u_{1I} + [(\lambda + 2\mu)\Phi_{IJ}^{(0,1)} n_2 + \mu\Phi_{IJ}^{(1,0)} n_1]u_{2I}\} \\
 & \quad -\epsilon_N < g(\mathbf{x}_J) > v_2 + \mu\epsilon_N < g(\mathbf{x}_J) > \text{sign}(\mathbf{u} \cdot \boldsymbol{\tau})\tau_2 = 0,
 \end{aligned} \tag{14}$$

where  $\mathbf{x}_J$  belongs to contact nodes on  $\Gamma_c$  and  $H(g)$  is the Heaviside function. Notice that the system of the equation is nonlinear due to the presence of contact constraints in (13) and (14). To use a full Newton-Raphson iteration scheme as a nonlinear solver, the residual of the system can be obtained by assembling the discrete forms of Dirichlet and Neumann boundary conditions, (12), and (13) for stick and (14) for slip. The tangent stiffness matrix can be computed by linearizing (13) for stick and (14) for slip. Notice that (13) and (14) can be used for both one- and two-body frictional contact with the proper definition of the gap function  $g(\mathbf{x})$ . The detailed procedure for the nonlinear solver can be found in Sect. 4 of [5].

## 2 Applications Including Frictional Contact

The method described in the previous section has several advantages due to the nature of the meshfree collocation method. The distinct feature of the method is an easy treatment of adaptive refinement because it does not require grid or mesh structure and numerical integration along with mesh connectivity. As a result, the method can simplify modeling of engineering problems requiring high accuracy locally. Another advantage of the method is the computation of higher-order derivative approximations without further cost. Using such derivative approximations, the method can easily evaluate a strong form of any order at spatially distributed collocation points. Upon making use of such advantages of the method, it has been further developed and applied to various engineering problems. The brief overview of the recent progress is provided in this section.

We first begin by reviewing the accuracy and efficiency of the method which has been performed by few researchers. Kim and Kim [1] provided  $L^2$ -convergence studies for Poisson and Stokes problems on both uniformly and non-uniformly distributed collocation points. The accuracy was tested for three values of the Taylor polynomial order, i.e.,  $m = 2, 3, 4$ , with varying the domain of influence  $\rho$ . For the Poisson problem, while no significant difference with  $m = 2$  and  $m = 3$  was observed, relatively higher accuracy was obtained for  $m = 4$ . For the Stokes problem, the same accuracy was observed in both velocity and pressure with  $m = 4$  as shown in Fig. 1a. Another

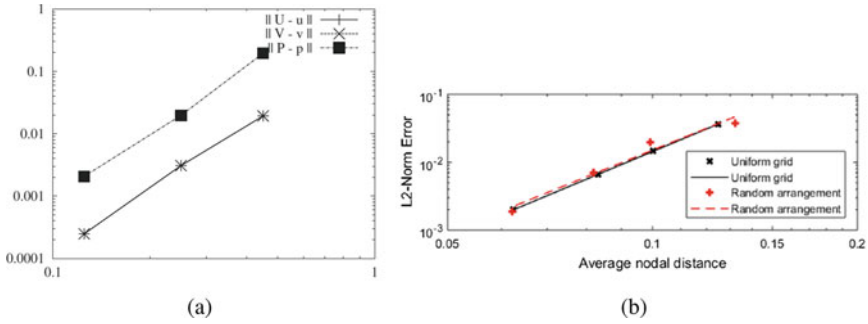


**Fig. 1** Convergence studies: **a** Stokes flow [1] and **b** Large-scale wind driven ocean circulation [6]

convergence study was performed by Beel et al. [6] for the large-scale wind driven ocean circulation problems in both the discrete  $L^2$ - and  $L^\infty$ -norm. They observed that the order of the convergence rate is approximately close to the order of the Taylor expansion without the boundary layer for both uniform and non-uniformly distributed collocation points as shown in Fig. 1b. On the other hand, with the presence of the boundary layer, low convergence rates and largely unpredictable error behavior were observed for randomly distributed collocation points (see Figs. 12 and 13 in [6]).

The computational efficiency of the meshfree collocation method was studied by Song et al. [7]. They used PETSc for parallel computing and performed numerical study of the polycrystalline solidification process. The computational time of the method was compared with that of the finite-difference method. They observed that the meshfree collocation method is more computationally demanding at each time step when compared with the finite-difference method. This is because the method requires sufficient amount of nodes within the compact support to ensure the invertibility of the moment matrix  $\mathbf{M}$ . However, relatively larger time step size with the method than the finite-difference method can be chosen, indicating that the difference between two methods becomes not significant.

An easy adaptive refinement of the method has been employed to various engineering problems to improve the accuracy of the solution. Almansí et al. [5] took advantage of the adaptivity to model frictional contact problems. The accuracy of the contact algorithm was examined for the frictional Hertzian contact by modeling a half cylinder compressed by both horizontal and vertical uniform displacement as shown in Fig. 15 of [5]. Collocation points were non-uniformly refined in the vicinity of the contact area where the stress is highly concentrated as shown in Fig. 2. The accuracy of the method was verified by comparing the normal and tangential tractions on the contact surface with the results from the finite-element method using ABAQUS (see Fig. 17 in [5]). Both tractions from the proposed collocation method are quantitatively close to those of the finite-element method.

Beel et al. [6] applied the advantage of the adaptive refinement to the large-scale wind driven ocean circulation problem. Both uniformly and non-uniformly

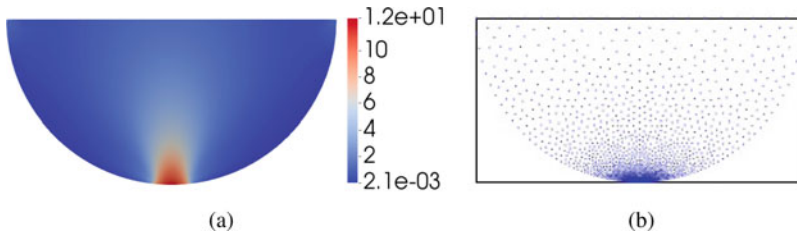


**Fig. 2** Adaptive refinement for frictional contact [5]: **a** Contour plot of the von mises stress and **b** Non-uniformly refined collocation points near contact area

collocation points were refined near the strong western boundary layer as shown in Fig. 14 of [6]. As summarized in Table 6 of [6], higher accuracy with uniform and non-uniform local refinements of collocation points was obtained than uniformly and non-uniformly distributed collocation points without local refinement. In addition, the strong form used in this study was the fourth-order partial differential equation with the strong western boundary layer. They showed that a sixth-order Taylor polynomial instead of fourth- and fifth-order polynomials is necessary to obtain reliable solutions due to the presence of the western boundary layer.

Another application of the adaptive refinement was done by Lee et al. [8]. They used the uniformly refined collocation points near the crack tip for dynamic crack propagation as shown in Figs. 8 and 13 of [8]. Moreover, the topology change due to crack extension was modeled by simple addition and deletion of collocation points. Good agreement with the analytical solution in terms of dynamic energy release rate and the direction of crack growth was observed with a relatively small number of collocation points.

The meshfree collocation method has been also applied to a phase-field model. Fu et al. [7] employed the method to the three-dimensional time dependent phase-field model for modeling the solidification process of a polycrystalline material along with the temperature change due to the latent heat. The solidification of polycrystalline nickel (Ni) from undercooled melt was selected to demonstrate the robustness and flexibility of the method. In Fig. 3, we display the polycrystalline structure of Ni obtained using non-uniformly distributed collocation points in three-dimension.

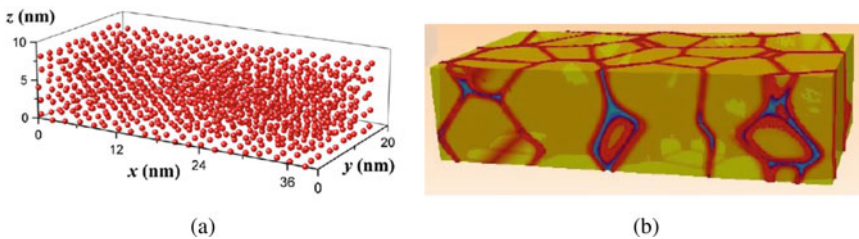


**Fig. 3** Polycrystalline solidification in three-dimension using a phase-field model [7]: **a** Non-uniformly distributed collocation points **b** Solidification of polycrystalline Ni

Furthermore, Almasi et al. [9] performed mechanical analysis of the polycrystalline materials using the polycrystalline structures obtained from the solidification simulation.

Further development and application of the method was done by Yoon and his colleagues. Yoon and Song [2–4] generalized the method to capture weak and strong discontinuities. This generalization was achieved by deriving the derivative approximation including enrichment terms to capture weak and strong discontinuities along the interface or moving boundary. The original derivative approximation (8) can be recovered without enrichment terms. Moreover, Yoon et al. [10] modeled simple material nonlinear problems by directly discretizing the force balance equation using the double derivative approximation without using the second-order derivative approximation. Yoon et al. [11] also applied the method for the simulation of a proportionally damped system subjected to dynamic load and the fracture simulation of cracked concrete beam.

**Acknowledgements** T.-Y. Kim gratefully appreciates the support from Khalifa University Internal Research Funding (CIRA-2019-009, No. 8474000170).

## References

1. Kim, D. W., & Kim, Y. S. (2003). Point collocation methods using the fast moving least square reproducing kernel approximation. *International Journal for Numerical Methods in Engineering*, *56*, 1445–1464.
2. Yoon, Y. C., & Song, J. H. (2014). Extended particle difference method for weak and strong discontinuity problems: Part I. Derivation of the extended particle derivative approximation for the representation of weak and strong discontinuities. *Computational Mechanics*, *53*, 1087–1103.
3. Yoon, Y. C., & Song, J. H. (2014). Extended particle difference method for weak and strong discontinuity problems: Part II. Formulations and applications for various interfacial singularity problems. *Computational Mechanics*, *53*, 1105–1128.
4. Yoon, Y. C., & Song, J. H. (2014). Extended particle difference method for moving boundary problems. *Computational Mechanics*, *54*, 723–743.
5. Almasi, A., Kim, T. Y., Laursen, T. A., & Song, J. H. (2019). A strong form meshfree collocation method for frictional contact on a rigid obstacle. *Computer Methods in Applied Mechanics and Engineering*, *357*, 112597.
6. Beel, A., Kim, T. Y., Jiang, W., & Song, J. H. (2019). Strong form-based meshfree collocation method for wind-driven ocean circulation. *Computer Methods in Applied Mechanics and Engineering*, *351*, 404–421.
7. Song, J. H., Fu, Y., Kim, T. Y., Yoon, Y. C., Michopoulos, J. G., & Rabczuk, T. (2018). Phase field simulations of coupled microstructure solidification problems via the strong form particle difference method. *International Journal of Mechanics and Materials in Design*, *14*, 491–509.
8. Lee, S. H., Kim, K. H., & Yoon, Y. C. (2016). Particle difference method for dynamic crack propagation. *International Journal of Impact Engineering*, *87*, 132–145.
9. Almasi, A., Beel, A., Kim, T. Y., Michopoulos, J. G., & Song, J. H. (2019). Strong-form collocation method for solidification and mechanical analysis of polycrystalline materials. *Journal of Engineering Mechanics*, *145*, 04019082.